# İNŞAAT MÜHENDİSLİĞİ ALANINDA AKADEMİK ANALİZLER

Editör: Doç. Dr. Emre TOPÇU

yaz yayınları

# İNŞAAT MÜHENDİSLİĞİ ALANINDA AKADEMİK ANALİZLER

**Editör**

Doç. Dr. Emre TOPÇU

yaz yayınları

**2024**

yaz
yayınları

# İNŞAAT MÜHENDİSLİĞİ ALANINDA AKADEMİK ANALİZLER

Editör: Doç. Dr. Emre TOPÇU

**© YAZ Yayınları**

Bu kitabın her türlü yayın hakkı Yaz Yayınları'na aittir, tüm hakları saklıdır. Kitabın tamamı ya da bir kısmı 5846 sayılı Kanun'un hükümlerine göre, kitabı yayınlayan firmanın önceden izni alınmaksızın elektronik, mekanik, fotokopi ya da herhangi bir kayıt sistemiyle çoğaltılamaz, yayınlanamaz, depolanamaz.

E_ISBN 978-625-6642-32-4

Mart 2024 – Afyonkarahisar

Dizgi/Mizanpaj: YAZ Yayınları

Kapak Tasarım: YAZ Yayınları

YAZ Yayınları. Yayıncı Sertifika No: 73086

M.İhtisas OSB Mah. 4A Cad. No:3/3
İscehisar/AFYONKARAHİSAR

www.yazyayinlari.com

yazyayinlari@gmail.com

info@yazyayinlari.com

# İÇİNDEKİLER

*"Bu kitapta yer alan bölümlerde kullanılan kaynakların, görüşlerin, bulguların, sonuçların, tablo, şekil, resim ve her türlü içeriğin sorumluluğu yazar veya yazarlarına ait olup ulusal ve uluslararası telif haklarına konu olabilecek mali ve hukuki sorumluluk da yazarlara aittir."*

# ZEMİN SIVILAŞMASININ DEĞERLENDİRİLMESİNDE ANALİTİK YÖNTEMLER

**Yusuf GÜZEL**[1]

## 1. GİRİŞ

Sıvılaşma, tamamen veya kısmen doygun zemin tabakalarında meydana gelen depremin sebep olduğu olaylardan biridir. Sıvılaşma fenomeni, sismik uyarılma sırasında zemin içerisinde hakim boşluk suyu basıncının artması nedeniyle zeminin dayanım ve rijitlik kaybı yaşaması olarak tanımlanabilir, bu da zeminin viskoz bir sıvı gibi davranmasına neden olur (Kramer, 1996). Zeminin sıvılaşma potansiyeli, zemin su seviyesi, tane şekilleri, gradasyon eğrisi, zeminin yoğunluğu, zemin tabakası kalınlığı, Standart Penetrasyon Testi darbe sayısı (SPT-N), Koni Penetrasyon Testi (CPT) ve kesme dalga hızı değerleri gibi faktörlere büyük ölçüde bağlılık göstermektedir (Kayabasi & Gokceoglu, 2018; Tunusluoglu & Karaca, 2018).

Sıvılaşma, sismik hareketlerden sonra veya sismik hareket sırasında kum kaynaması veya zeminde oturma sonucunda meydana gelen temel taşıma kapasitesi başarısızlıklarına, heyelanlara, yol çökmesine ve altyapı sistemlerinin hasar görmesine neden olabilir (Lirer, Chiaradonna, & Mele, 2020). Sıvılaşmaya bağlı benzer türdeki olaylar 1964 yılında, Alaska'da yaşanan Good Friday depremi ve Japonya'da meydana gelen Niigata depremi sonrasında gözlemlenmiştir (Kazama, Sento,

[1] Öğretim Görevlisi (Dr.), Necmettin Erbakan Üniversitesi, Mühendislik Fakültesi, İnşaat Mühendisliği, e-mail:yusufkurtdereli@hotmail.com, ORCID: 0000-0003-2957-8060.

Uzuoka, & Ishimaru, 2008; Rouholamin, Bhattacharya, & Orense, 2017; Sönmezer, Akyüz, & Kayabali, 2020). Daha yakın zamanlarda, 1992 Erzincan depremi (Isik, Unsal, Gurbuz, & Sisman, 2016), 1998 Adana-Ceyhan depremi (Ulusay ve Kuru, 2004), 1999 Izmit (Kocaeli) deprem olayı (Cetin et al., 2004; Sonmez & Ulusay, 2008), 1999 Düzce depremi (Yoshida, Tokimatsu, Yasuda, Kokusho, & Okimura, 2001), 2010 Christchurch depremi (Cubrinovski vd., 2010; Maurer, Green, Cubrinovski, & Bradley, 2014), 2012 Emilia depremi (Di Manna vd., 2012; Papathanassiou, Mantovani, Tarabusi, Rapti, & Caputo, 2015), 2018 Endonezya depremi (Sassa & Takagawa, 2019) gibi birçok deprem olayında sıvılaşma nedeni ile meydana gelen hasarlar gözlemlenmiştir. Son olarak 6 Şubat 2023 Kahramanmaraş depremlerinde de, Şekil 1'de görüldüğü gibi, sıvılaşma nedeni ile hasarlar meydana gelmiştir (Karabacak vd., 2023; Ozener, Monkul, Bayat, Ari, & Cetin, 2024).

**Şekil 1 Gölbaşı (Adıyaman) İlçesindeki Bir Binada Sıvılaşmadan Dolayı Meydana Gelen Oturma Durumu**

Sıvılaşma olayı, deprem riski taşıyan bölgelerdeki hakim olarak taneli zeminlerden oluşan zemin tabakalarında meydana

gelmesi mümkündür, çünkü sıvılaşma deprem ivme hareketleri tarafından tetiklenir. Deprem riski bulunan bölgelerin sıvılaşma potansiyelinin ortaya konması ve değerlendirilmesi, altyapı üzerinde oluşabilecek hasarların tespiti, sismik tehlike risklerini anlama ve gelecekteki yaşam alanlarını planlamak için önemlidir (Meisina vd., 2022; Zhang, Xie, Zhang, Qiu, & Wu, 2021). Sıvılaşma potansiyelinin değerlendirilmesi laboratuvar ve/veya saha testleri yoluyla yapılabilir. Laboratuvar testlerinde, zemin numuneleri in-situ koşullara getirilmeli (yani, Ko gerilmesi veya tabii gerilme koşulları) ve daha sonra torsiyonel kayma veya üç eksenli testlere tabi tutulmalıdır, ki bu başlangıçta Seed ve Lee (1966) tarafından önerilmiştir. Bu laboratuvar testlerinin zemin numunelerinin sıvılaşma potansiyelini tahmin etme üzerindeki çeşitli yönleri, Tatsuoka ve Silver (1981), Kokusho, Yoshida, Nishi, and Esashi (1983), Yamashita ve Toki (1993), Idriss ve Boulanger (2006) tarafından incelenmiştir.

Ancak, laboratuvar ortamlarında in-situ koşullarının elde edilmesi zor olabilir. Ayrıca, uygun şekillerde tahribatsız zemin numunesinin alınması ve uygun şartlarda laboratuvar ortamına taşınması ve test düzeneğine yerleştirilmesi gibi durumlar laboratuvar deneyinde karşılaşılan başlıca zorluklardır. Bu nedenle, Standart Penetrasyon Testi (SPT), Koni Penetrasyon Testi (CPT) kesme dalga hızı (Vs) ölçüm yöntemleri gibi saha testleri, zemin sıvılaşmasının değerlendirilmesi için daha güvenilir olarak kabul edilir (Clayton, Hight, & Hopper, 1992; Hight, Boese, Butcher, Clayton, & Smith, 1992). Bu saha testlerinden elde edilen zemin verilerine bağlı geliştirilen yöntemler, çeşitli çalışmalarda (Akkaya, Ozvan, Akin, Akin, & Ovun, 2018; Dobry et al., 2015; Muley, Maheshwari, & Kirar, 2022; Toprak, Holzer, Bennett, & Tinsley III, 1999; Vipin, Sitharam, & Anbazhagan, 2010) farklı bölgelerin sıvılaşma potansiyelini değerlendirmek için yaygın olarak uygulanmıştır.

## 2. BASİTLEŞTİRİLMİŞ SIVILAŞMA DEĞERLENDİRME YÖNTEMLERİ

### 2.1. Standard Penetrasyon Testine Bağlı Sıvılaşma Değerlendirme Yöntemi

Genellikle sıvılaşma analizi yapılacak bir sahada zeminin mekanik özelliklerini çok iyi derecede yansıtan standart penetrasyon testi (SPT) yapılmış olmaktadır. Bu nedenle, SPT darbe sayısınına bağlı analitik sıvılaşma yöntemleri geliştirilmiştir. Dünya genelinde yaygın olarak kullanılan analitik metot Seed ve Idriss (1971) tarafından geliştirilmiş ve ardından Seed, Tokimatsu, Harder, ve Chung (1985) tarafından modifiye edilmiştir. Bu analitik yöntemde ilk aşama SPT darbe sayısının ($N_{30}$) düzeltilmesidir. Bu düzeltme işlemi aşağıda verilen formül ile gerçekleştirilmektedir (Youd vd., 2001):

$$(N_1)_{60} = N_m C_N C_E C_B C_R C_S \quad (1)$$

Burada, $N_m$: ölçülen darbe sayısı, $C_N$: kohezyonsuz zeminlerde uygulanan derinlik düzeltme katsayısını, $C_E$: enerji oranı düzeltme katsayısını, $C_R$: tij boyu düzeltme katsayısını, $C_S$: numune alıcı düzeltme katsayısını göstermektedir. Derinlik düzeltme katsayısı Liao and Whitman (1986) tarafından verilen Denklem 2'e göre hesaplanacaktır:

$$C_N = \left(\frac{P_a}{\sigma'_{vo}}\right)^{0.5} \quad (2)$$

Denklem 2, $P_a$ atmosfer basıncını (100 kPa=1 atm) ve $\sigma'_{vo}$düşey efektif gerilmeyi ifade etmektedir. Derinlik düzeltme katsayısı 1.70 değerinden büyük olamaz. Bunun yanında, kumlu zeminlerin içerisindeki ince tane içeriği (IDI) zeminin sıvılaşma direncini etkilediğinden dolayı, IDI'ya bağlı olarak Denklem 3'ten elde edilen $(N_1)_{60}$ değeri Denklem 3'e göre düzeltilmelidir.

$$(N_1)_{60cs} = \alpha + \beta(N_1)_{60} \quad (3)$$

Burada, $\alpha$ ve $\beta$ katsayıları IDI oranına bağlı olarak aşağıdaki şekilde ifade edilmektedir:

$$\begin{aligned} &IDI \leq \%5, && \alpha = 0 \; and \; \beta = 1 \\ &\%5 < IDI \leq \%35, && \alpha = \exp\left[1.76 - \left(\tfrac{190}{IDI^2}\right)\right] \; and \; \beta = [0.99 + (\tfrac{IDI^{1.5}}{1000})] \\ &IDI \geq \%35, && \alpha = 5 \; and \; \beta = 1.2 \end{aligned} \quad (4)$$

Bir zeminin sıvılaşma potansiyelini belirlemek için çevrimsel dayanım oranının (CRR) ve depremin oluşturabileceği çevrimsel gerilme oranının (CSR) hesaplanması gerekmektedir. Tanım olarak, CRR, zeminde sıvılaşmaya karşı direnci gösterirken, CSR herhangi bir potansiyel deprem olayı sırasında zemin içindeki kayma gerilim seviyesini ifade etmektedir.

CRR ve CSR'nin hesaplanması için formülasyonlar Seed vd. (1985) tarafından aşağıdaki denklemlerle verilmiştir:

$$CRR_{7.5} = \frac{1}{34 - (N_1)_{60}} + \frac{(N_1)_{60}}{135} + \frac{50}{[10(N_1)_{60} + 45]^2} - \frac{1}{200} \quad (5)$$

$$CSR = 0.65(\tfrac{\alpha_{max}}{g})(\tfrac{\sigma_{vo}}{\sigma'_{vo}})r_d \quad (6)$$

Bu denklemlerde, $\alpha_{max}$ maksimum zemin ivme değerini (PGA), $g$ yerçekimi ivme değerini, $\sigma_{vo}$and $\sigma'_{vo}$ toplam ve efektif düşey gerilmeleri ve $r_d$ gerilme azaltma katsayısını göstermektedir. Gerilme azaltma katsayısı,$r_d$, derinliğe bağlı aşağıda verilen denklemler ile hesaplanmaktdır (Seed & Idriss, 1971):

$$\begin{aligned} r_d &= 1 - 0.00765z && z \leq 9.15\ m \\ r_d &= 1.174 - 0.0267z && 9.15\ m < z \leq 23\ m \\ r_d &= 0.744 - 0.008z && 23\ m < z \leq 30\ m \end{aligned} \quad (7)$$

Son olarak, sıvılaşmaya karşı güvenlik katsayısı (Gs) aşagıdaki formül kullanılarak elde edilmektedir (Youd vd., 2001):

$$Gs = ({}^{CRR_{7.5}}/_{CSR})\text{MSF} \quad (8)$$

MSF, deprem büyüklüğü düzeltme katsayısı aşağıda verilen Denklem 9 ile hesaplanmaktadır.

$$MSF = \frac{10^{2.24}}{M_w^{2.56}} \quad (9)$$

### 2.2. Kesme Dalga Hızına Bağlı Sıvılaşma Değerlendirme Yöntemi

Bu yöntemde de, bir önceki yöntemde olduğu gibi çevrimsel dayanım oranının (CRR) ve depremin oluşturabileceği çevrimsel gerilme oranının (CSR) hesaplanması gerekmektedir. Fakat burada SPT deney verileri yerine çok kanallı yüzey dalga, sismik kırılma, mikrotremor veya düşey elektrik sondaj çalışmaları ile elde edilen kesme dalga hızı kullanılmaktadır.

Sıvılaşmaya karşı zeminin güvenlik katsayısı Denklem 10'de verilmektedir (Uyanık, Ekinci, & Uyanik, 2013).

$$Gs_{Vs} = \frac{CRR_{Vs}}{CSR_{Vs}} = \frac{SRR}{SSR} \tag{10}$$

Denklem 10'de SRR kayma direnci oranının ifade ederken SSR kayma gerilmesi oranını temsil etmektedir. SRR değerinin hesaplanması için $V_s$ değerlerinin aşağıda ifade edilen formüle göre düzeltilmelidir.

$$V_{s_c} = V_s \left(\frac{P_a}{\sigma'_{vo}}\right) \tag{11}$$

Burada, $\sigma'_{vo}$ zemin düşey efektif gerilmeyi (kPa), $V_{s_c}$ düzeltilmiş $V_s$ değerini ve $P_a$ atmosferik basıncı (100 kPa olarak kabul edilmektedir) ifade eder. $V_{s_c}$ değerinin hesaplanması ile birlikte SRR değeri Denklem 12'ye göre bulunmaktadır (Andrus & Stokoe II, 2000; Uyanık & Taktak, 2009; Youd vd., 2001).

$$SRR = \left[a\left(\frac{V_{s_c}}{100}\right)^2 + b\left(\frac{1}{V_{s_{mak}} - V_{s_c}} - \frac{1}{V_{s_{mak}}}\right)\right] MSF \tag{12}$$

$$V_{s_{mak}} = 250\ {}^{m}/_{s} \qquad IDI \leq \%5$$

$$V_{s_{mak}} = 250 - (IDI - 5)\ {}^{m}/_{s} \qquad \%5 \leq \text{IDI} \leq \%35$$

$$V_{s_{mak}} = 220\ {}^{m}/_{s} \qquad IDI \geq \%35 \tag{13}$$

Andrus ve Stokoe (2000) $V_{s_{mak}}$ değeri için 215 m/s ve $a$ ve $b$ regresyon katsayıları için sırası ile 0.022 ve 2.8 değerlerini önermektedir. Bunun yanında Uyanık (2006) bu parametreler için

sırası ile 250 m/s, 0.025 ve 4 değerlerini ortaya koymaktadır. Deprem büyüklüğü düzeltme katsayısı, MSF, deprem büyüklüğüne bağlı olarak Denklem 14'e göre hesaplanmaktadır.

$$MSF = \left(\frac{M_w}{7.5}\right)^n \quad (M_w > 7.5\ ise\ n = -2.56 \qquad M_w \leq 7.5\ ise\ n = -3.3) \tag{14}$$

SSR değerinin $V_s$ değerine bağlı olarak hesaplanması Seed ve Idriss (1971) tarafından öne sürülmüş ve Uyanık vd. (2013) tarafından modifiye edilmiştir.

$$SSR = ({}^{\alpha_{mak}}/_{g})({}^{\sigma_{V_s}}/_{\sigma'_{V_s}})r_d \tag{15}$$

$$\sigma_{V_s} = 0.25T\sum_{i=1}^{n}\gamma_i V_{si}$$

$$\sigma'_{V_s} = \sigma_{V_s} - u = 0.25T\left(\sum_{i=1}^{n}\gamma_i V_{si} - V_{sn}(\gamma_{sat} - \gamma_d)\right) \tag{16}$$

Denklem 16'da $\alpha_{mak}$ maksimum yatay zemin ivmesini (m/s$^2$), g yerçekimi ivmesini (m/s$^2$), $\sigma_{V_s}$ inceleme deriliğindeki dinamik düşey gerilmeyi (kN/m$^2$), $\sigma'_{V_s}$ inceleme derinliğindeki dinamik düşey gerilmeyi (kN/m$^2$), $r_d$ Denklem 9'da hesaplanan gerilme azaltma katsayısını temsil etmektedir. Ayrıca, $T$ deprem dalgasının hakim periyotunu (s), n sıvılaşma potensiyeli olan katmanı ve bu katmandaki tabaka sayısını, $V_{si}$ herbir zemin tabakasındaki kesme dalga hızını (m/s), $\gamma_i$ zeminin birim hacim ağırlığını (kN/m$^3$), $\gamma_{sat}$ zeminin suya doygun durumdaki birim hacim ağırlığını (kN/m$^3$) ve $\gamma_d$ zeminin kuru birim hacim ağırlığını (kN/m$^3$) göstermektedir.

Farklı büyüklükteki depremlerin 50 km ve üzeri merkez üstü mesafelerindeki hakim periyotları Çizelge 1'de gösterilmiştir. Çizelgeden görüldüğü üzere, hakim periyot deprem büyüklüğünün azalması ile birlikte azalmaktadır.

*Çizelge 1 Farklı deprem büyüklüklerine göre merkezüstüne 50 km ve üzerinde bulunan sahalar için önerilen hakim periyot değerleri (Uyanık & Taktak, 2009)*

| M | 7.7 | 7.6 | 7.5 | 7.4 | 7.3 | 7.3 | 7.1 | 7.0 | 6.9 | 6.8 |
|---|---|---|---|---|---|---|---|---|---|---|
| T(s) | 0.379 | 0.364 | 0.350 | 0.348 | 0.347 | 0.33 | 0.322 | 0.307 | 0.302 | 0.301 |
| M | 6.7 | 6.6 | 6.5 | 6.4 | 6.3 | 6.2 | 6.1 | 6.0 | 5.9 | |
| T(s) | 0.291 | 0.285 | 0.280 | 0.275 | 0.269 | 0.264 | 0.256 | 0.253 | 0.250 | |

### 2.3. Koni Penetrasyon Deneyine Bağlı Sıvılaşma Değerlendirme Yöntemi

Koni penetrasyon deneyi (CPT), zeminin özelliklerini belirlemede sıkça kullanılan bir saha deneyidir. Bu deney, zemin profilinin tamamı boyunca bilgi edinilmesini sağladığı için tercih edilebilir. CPT deneyleri ile elde edilen veriler genellikle uç sürtünme direnci ($q_c$), çevresel sürtünme değeri ($f_s$) ve sürtünme oranı (F) olarak doğrudan tanımlanır.

Sıvılaşma analizlerinde koni penetrasyon arazi deneyinden elde edilen verilere bağlı olarak çevrimsel dayanım oranı (CRR) hesaplanmaktadır. Temiz (saf) kum için önerilen CRR değeri aşağıda verilen denklemler ile tahmin edilebilir (Robertson & Wride, 1998):

$$(q_{c1N})_{CS} < 50 \; ise \; CRR_{7.5} = 0.833 \left[\frac{(q_{c1N})_{CS}}{1000}\right] + 0.05$$

$$50 \leq (q_{c1N})_{CS} < 160 \; ise \tag{17}$$

$$CRR_{7.5} = 93 \left[\frac{(q_{c1N})_{CS}}{1000}\right]^3 + 0.08$$

Denklem 17'de $(q_{c1N})_{CR}$ temiz kum için 100 kPa değeri ile normalize edilmiş uç sürtünme direncini ifade etmektedir. Boyutsuz $q_{c1N}$ değeri aşağıdaki formüllere göre belirlenmektedir.

$$q_{c1N} = C_Q(\frac{q_c}{P_a}) \tag{18}$$

$$C_Q = (\frac{P_a}{\sigma'_{vo}})^n \tag{19}$$

Bu denklemlerde $C_Q$ uç sürtünme direnci normalize faktörünü, $P_a$ atmosferik basıncını (1 atm), $\sigma'_{vo}$ efektif düşey gerilmeyi, $n$ zemin cinsine bağlı değişken katsayısını, $q_c$ uç sürtünme direncini ifade etmektedir. $C_Q$ değeri zemin yüzeyine yakın derinliklerde düşey efektif gerilmenin düşük olmasından dolayı büyük olabilir. Fakat bu değer 1.7 değerini aşamaz. Zemin cisine göre değişkenlik gösteren n ise kum için 0.5 iken kil için 1 değerini almaktadır (Olsen, 1997). Silt veya siltli kumlar için n 0.5 ila 1 arasında değerler almaktadır.

Sürtünme oranı (F) çevresel sürtünme direncinin uç direncine oranına eşittir ve genelde ince dane oranının ve zemin plastisitesinin artması ile birlikte artış göstermektedir. Bu nedenle sürtünme oranı zemin içeriği ve zemin cinsi hakkında bilgi sağlayabilir. CPT verileri ile birlikte zemin davranışını dikkate alarak zemin davranış cinsi indeks değeri $(I_c)$ öne sürülmüştür (Robertson & Wride, 1998). Bu değer Denklem 20 ve takibindeki ilgili formüllerle hesaplanmaktadır.

$$I_c = [(3.47 - logQ)^2 + (1.22 + logF)^2]^{0.5} \tag{20}$$

$$Q = [(q_c - \sigma_{vo})/P_a][(P_a/\sigma'_{vo})^n] \tag{21}$$

$$F = [f_s/(q_c - \sigma_{vo})] \times 100\% \tag{22}$$

Eğer n katsayısı (Denklem 21) 1 kabul edilip $I_c$ değeri 2.6'nın üzerinde elde edilirse zemin killi kabul edilir ve sıvılaşma durumu beklenmediği için sıvılaşma analizi tamamlanmış olur. Gerçekte ince taneli zemin içeren herhangi bir granüllü zeminde sıvılaşmadan söz edilebilmesi için şu üç şartın sağlanması gerekmektedir (H Bolton Seed & Idriss, 1982):

- Kil içeriğinin ağırlıkça %15'ten az olması,
- Likit limitin %35'ten küçük olması ve
- Doğal su içeriğinin likit limit değerinin 0.9'undan büyük olması.

Fakat n değerinin 1 kabul edildiği durumda $I_c$ değeri 2.6'dan küçük bulunursa, zeminin büyük olasılıkla granüllü bir yapıya sahip olduğu düşünülür. Bu durumda, $C_Q$ ve $Q$ katsayıları n katsayısı 0.5 kabul edilerek tekrar hesaplanır. Bu kabul ile birlikte $I_c$ değeri halen 2.6'dan küçük ise zemin plastik olmayan granüllü olarak tanımlanır. $I_c$ değeri 2.6'dan büyük bulunursa zemin silt içerikli ve dolayısı ile plastik olarak düşünülür. Böylece, $q_{c1N}$ (Denklem 18) dikkate alınarak ve n değeri 0.7 alınarak hesaplanır. Fakat burada zemin numunesi alınarak incelenmeli ve yukarıda Seed & İdriss (1982) tarafından belirtilen maddelere bakılması gerekmektedir.

Siltli kumlar için elde edilen normalize edilmiş uç sürtünme direnci eşdeğer sade kum için olan eşdeğer değeri Denklem 23'e göre hesaplanır.

$$(q_{c1N})_{CS} = K_c q_{c1N} \tag{23}$$

Burada $K_c$ granül tane karakteristiği için düzeltme katsayısını ifade eder ve şu şekilde hesaplanır (Robertson & Wride, 1998):

$$I_c \leq 1.64 \text{ ise } K_c = 0 \tag{24}$$

$$I_c > 1.64 \text{ ise } K_c = -0.403I_c^4 + 5.581I_c^3 - 21.63I_c^2 + 33.75I_c - 17.88$$

## 3. SONUÇ

Bir sahada sıvılaşma potansiyelinin ortaya konması potansiyel deprem risk analizi ve değerlendirilmesi ile birlikte gelecek şehir planlaması açısından da büyük önem arz etmektedir. Saha deneyleri ile elde edilen verilerin sıvılaşma potansiyelinin değerlendirilmesinde kullanılması, direk olarak sahada zemin hakkında bilgi verdiği için, çoğu zaman tercih edilmiş ve bunlar üzerine yöntemler geliştirilmiştir. En çok kullanılan saha deneyleri standart penetraston testi (SPT), koni penetrasyon testi (CPT) ve çok kanallı yüzey dalga, sismik kırılma gibi kesme dalga hızının elde edildiği testlerdir. Bu testlere dayalı sıvılaşma değerlendirme yöntemleri bu bölümde sunulmuştur.

Burada ifade edilmelidir ki, sıvılaşma olayı deprem ivme hareketi ile tetiklendiğinden dolayı, esasında sıvılaşmanın gerçekleşme durumunu olasılıksal olarak ifade etmek daha kapsamlı bir yaklaşım olacaktır. Çünkü, depremin nerede, ne zaman ve hangi büyüklükte gerçekleşeceği deterministik değil olasılı bir durumdur. Ayrıca sahada elde edilen veriler de belirli bir değişkenliğe sahiptir. Bundan dolayı sıvılaşma potansiyelinin değerlendirilmesi için bahsedilen olasılık durumlarını içine alan yöntemler de son zamanlarda geliştirilmektedir. Yine de basitleştirilmiş yöntemler sıvılaşma potansiyeli değerlendirmesindeki yerini korumaktadır.

## KAYNAKÇA

Akkaya, I., Ozvan, A., Akin, M., Akin, M. K., & Ovun, U. (2018). Comparison of SPT and V-s-based liquefaction analyses: a case study in Ercis (Van, Turkey). *Acta Geophysica, 66*(1), 21-38. doi:10.1007/s11600-017-0103-0

Andrus, R. D., & Stokoe II, K. H. (2000). Liquefaction resistance of soils from shear-wave velocity. *Journal of geotechnical geoenvironmental engineering, 126*(11), 1015-1025.

Cetin, K. O., Seed, H. B., Der Kiureghian, A., Tokimatsu, K., Harder, L., Kayen, R., & Moss, R. (2004). SPT-Based probabilistic and deterministic assessment of seismic soil liquefaction potential. *Journal of Geotechnical and Geoenvironmental Engineering, 130*(12), 1314-1340. doi:10.1016/j.dib.2018.08.043

Clayton, C. R. I., Hight, D. W., & Hopper, R. J. (1992). Progressive destructuring of bothkennar clay - implications for sampling and reconsolidation procedures. *Geotechnique, 42*(2), 219-239. doi:10.1680/geot.1992.42.2.219

Cubrinovski, M., Green, R., Allen, J., Ashford, S., Bowman, E., Bradley, B.,……, Orense, R. (2010). *Geotechnical reconnaissance of the 2010 Darfield (New Zealand) earthquake*. *Bulletin of New Zealand Society of Earthquake Engineering, 43(4)*, 243-320.

Di Manna, P., Guerrieri, L., Piccardi, L., Vittori, E., Castaldini, D., Berlusconi, A., . . . Gambillara, R. (2012). Ground effects induced by the 2012 seismic sequence in Emilia: implications for seismic hazard assessment in the Po Plain. *Annals of Geophysics*. doi:10.4401/ag-6143

Dobry, R., Abdoun, T., Stokoe, K. H., Moss, R. E. S., Hatton, M., & El Ganainy, H. (2015). Liquefaction Potential of Recent

Fills versus Natural Sands Located in High-Seismicity Regions Using Shear-Wave Velocity. *Journal of Geotechnical and Geoenvironmental Engineering, 141*(3). doi:10.1061/(asce)gt.1943-5606.0001239

Hight, D. W., Boese, R., Butcher, A. P., Clayton, C. R. I., & Smith, P. R. (1992). Disturbance of the bothkennar clay prior to laboratory testing. *Geotechnique, 42*(2), 199-217. doi:10.1680/geot.1992.42.2.199

Idriss, I. M., & Boulanger, R. W. (2006). Semi-empirical procedures for evaluating liquefaction potential during earthquakes. *Soil Dynamics and Earthquake Engineering, 26*(2-4), 115-130. doi:10.1016/j.soildyn.2004.11.023

Isik, A., Unsal, N., Gurbuz, A., & Sisman, E. (2016). Assessment of liquefaction potential of fethiye based on spt and shear wave velocity. *Journal of the Faculty of Engineering and Architecture of Gazi University, 31*(4), 1027-1037. doi:10.17341/gazimmfd.278458

Karabacak, V., Özkaymak, Ç., Sözbilir, H., Tatar, O., Aktug, B., Özdag, Ö., . . . Arslan, G. (2023). The 2023 Pazarck (Kahramanmaras, Turkiye) earthquake (Mw 7.7): implications for surface rupture dynamics along the East Anatolian Fault Zone. *Journal of the Geological Society, 180*(3). doi:10.1144/jgs2023-020

Kayabasi, A., & Gokceoglu, C. (2018). Liquefaction potential assessment of a region using different techniques (Tepebasi, Eskişehir, Turkey). *Journal of Environmental earth sciences, 246*, 139-161.

Kazama, M., Sento, N., Uzuoka, R., & Ishimaru, M. (2008, May 30-Jun 02). *Progressive damage simulation of foundation pile of the Showa bridge caused by lateral spreading during the 1964 Niigata earthquake.* Paper presented at

the 2nd International Conference for Disaster Mitigation and Rehabilitation, Nanjing, PEOPLES R CHINA.

Kokusho, T., Yoshida, Y., Nishi, K., & Esashi, Y. (1983). *Evaluation of seismic stability of dense sand layer (Part 1)-Dynamic strength characteristics of dense sand*. CRIEPI Report, Central Research Institute of Electric Power Industry.

Kramer, S. L. (1996). *Geotechnical earthquake engineering*: Pearson Education India.

Lirer, S., Chiaradonna, A., & Mele, L. (2020). Soil Liquefaction: from mechanisms to effects on the built environment. *Italian Geotechnical Journal-Rivista Italiana Di Geotecnica, 54*(3), 23-51. doi:10.19199/2020.3.0557-1405.023

Maurer, B. W., Green, R. A., Cubrinovski, M., & Bradley, B. A. (2014). Evaluation of the liquefaction potential index for assessing liquefaction hazard in Christchurch, New Zealand. *Journal of Geotechnical and Geoenvironmental Engineering, 140*(7), 04014032. doi:10.1061/(ASCE)GT.1943-5606.0001117

Meisina, C., Bonì, R., Bozzoni, F., Conca, D., Perotti, C., Persichillo, P., & Lai, C. G. (2022). Mapping soil liquefaction susceptibility across Europe using the analytic hierarchy process. *Bulletin of Earthquake Engineering, 20*(11), 5601-5632. doi:10.1007/s10518-022-01442-8

Muley, P., Maheshwari, B. K., & Kirar, B. (2022). Liquefaction Potential of Sites in Roorkee Region Using SPT-Based Methods. *International Journal of Geosynthetics and Ground Engineering, 8*(2). doi:10.1007/s40891-022-00374-2

Olsen, R. S. (1997). *Cyclic liquefaction based on the cone penetration test.* Paper presented at the NCEER Workshop on Evaluation of Liquefaction Resistance of Soils, State Unıversıty of New York.

Ozener, P., Monkul, M. M., Bayat, E. E., Ari, A., & Cetin, K. O. (2024). Liquefaction and performance of foundation systems in Iskenderun during 2023 Kahramanmaras-Turkiye earthquake sequence. *Soil Dynamics Earthquake Engineering Research Institute Monograph Series, 178*, 108433.

Papathanassiou, G., Mantovani, A., Tarabusi, G., Rapti, D., & Caputo, R. (2015). Assessment of liquefaction potential for two liquefaction prone areas considering the May 20, 2012 Emilia (Italy) earthquake. *Journal of Environmental earth sciences, 189*, 1-16. doi:10.1016/j.enggeo.2015.02.002

Robertson, P. K., & Wride, C. E. (1998). Evaluating cyclic liquefaction potential using the cone penetration test. *Canadian Geotechnical Journal, 35*(3), 442-459. doi:10.1139/t98-017

Rouholamin, M., Bhattacharya, S., & Orense, R. P. (2017). Effect of initial relative density on the post-liquefaction behaviour of sand. *Soil Dynamics and Earthquake Engineering, 97*, 25-36. doi:10.1016/j.soildyn.2017.02.007

Sassa, S., & Takagawa, T. (2019). Liquefied gravity flow-induced tsunami: first evidence and comparison from the 2018 Indonesia Sulawesi earthquake and tsunami disasters. *Landslides, 16*(1), 195-200. doi:10.1007/s10346-018-1114-x

Seed, H. B., & I.M., I. (1971). Simplified Procedure for Evaluating Soil Liquefaction Potential. *Journal of the Soil Mechanics and Foundation Divisions, 97*(SM9), 1249-1273. doi:10.1061/JSFEAQ.0001662

Seed, H. B., & Idriss, I. (1982). *Ground motion and soil liquefaction during earthquakes*.

Seed, H. B., & Idriss, I. M. (1971). Simplified procedure for evaluating soil liquefaction potential. *Journal of the Soil Mechanics Foundations division, 97*(9), 1249-1273.

Seed, H. B., & Lee, K. (1966). Liquefaction of saturated sands during cyclic loading. *Journal of the Soil Mechanics*

*Foundations Division, 92*(6), 105-134.

Seed, H. B., Tokimatsu, K., Harder, L. F., & Chung, R. M. (1985). Influence of SPT procedures in soil liquefaction resistance evaluations. *Journal of Geotechnical Engineering-Asce, 111*(12), 1425-1445.

Sonmez, B., & Ulusay, R. (2008). Liquefaction potential at Izmit Bay: comparison of predicted and observed soil liquefaction during the Kocaeli earthquake. *Bulletin of Engineering Geology and the Environment, 67*(1), 1-9. doi:10.1007/s10064-007-0105-2

Sönmezer, Y. B., Akyüz, A., & Kayabali, K. (2020). Investigation of the effect of grain size on liquefaction potential of sands. *Geomechanics and Engineering, 20*(3), 243-254. doi:10.12989/gae.2020.20.3.243

Tatsuoka, F., & Silver, M. L. (1981). Undrained stress-strain behavior of sand under irregular loading. *Soils and Foundations, 21*(1), 51-66.

Toprak, S., Holzer, T., Bennett, M. J., & Tinsley III, J. C. (1999). *CPT-and SPT-based probabilistic assessment of*

*liquefaction.* Paper presented at the Proc., 7th US–Japan Workshop on Earthquake Resistant Design of Lifeline Facilities and Countermeasures against Liquefaction, Buffalo, NY.

Tunusluoglu, M. C., & Karaca, O. (2018). Liquefaction severity mapping based on SPT data: a case study in Canakkale city (NW Turkey). *Journal Environmental earth sciences, 77*(12), 1-29. doi:10.1007/s12665-018-7597-x

Uyanık, O. (2006). Sıvılaşır yada sıvılaşmaz zeminlerin yinelemeli gerilme oranına bir seçenek. *DEÜ Mühendislik Fakültesi Fen ve Mühendislik Dergisi, 8*(2), 79-91.

Uyanık, O., Ekinci, B., & Uyanik, N. A. (2013). Liquefaction analysis from seismic velocities and determination of lagoon limits Kumluca/Antalya example. *Journal of Applied Geophysics, 95*, 90-103. doi:10.1016/j.jappgeo.2013.05.008

Uyanık, O., & Taktak, A. G. (2009). Kayma Dalga Hızı ve Etkin Titresim Periyodundan Sıvılasma Çözümlemesi için Yeni Bir Yöntem. *Süleyman Demirel Üniversitesi Fen Bilimleri Enstitüsü Dergisi, 13*(1), 74-81.

Vipin, K. S., Sitharam, T. G., & Anbazhagan, P. (2010). Probabilistic evaluation of seismic soil liquefaction potential based on SPT data. *Natural Hazards, 53*(3), 547-560. doi:10.1007/s11069-009-9447-3

Yamashita, S., & Toki, S. (1993). Effects of fabric anisotropy of sand on cyclic undrained triaxial and torsional strengths. *Soils and Foundations, 33*(3), 92-104.

Yoshida, N., Tokimatsu, K., Yasuda, S., Kokusho, T., & Okimura, T. (2001). Geotechnical aspects of damage in Adapazari City during 1999 Kocaeli, Turkey earthquake.

*Soils and Foundations, 41*(4), 25-45. doi:10.3208/sandf.41.4_25

Youd, T. L., Idriss, I. M., Andrus, R. D., Arango, I., Castro, G., Chritrian, J., . . . al., e. (2001). Liquefaction resistance of soils: summary report from the 1996 NCEER and 1998 NCEER/NSF workshops on evaluation of liquefaction resistance of soils. *Journal of Geotechnical and Geoenvironmental Engineering, 127*(10), 817-833. doi:10.1061/(ASCE)1090-0241(2001)127:10(817)

Zhang, Y., Xie, Y., Zhang, Y., Qiu, J., & Wu, S. (2021). The adoption of deep neural network (DNN) to the prediction of soil liquefaction based on shear wave velocity. *Journal of Bulletin of Engineering Geology and the Environment, 80*(6), 5053-5060.

# DROUGHT ANALYSIS USING COMPOSITE DROUGHT INDEX (CDI) IN ISTANBUL

**Emre TOPÇU**[1]

**Fatih KARAÇOR**[2]

## 1. INTRODUCTION

Drought is a natural climatic phenomenon of concern for humans, whose body is 65% water, and for all vital and physical phenomena on Earth. Drought does not have a precise definition. Defining drought precisely is a challenge for researchers due to variations in hydrometeorological parameters, socioeconomic factors, and water demands across different geographical regions. Drought definitions are mostly regional and may not reflect the drought situation in other regions. However, we can still define drought as "a statistically periodic lack of rainfall and soil water in a region". In general terms, we can say that drought occurs when the amount of precipitation falling in a particular region is much lower than the long-term average of that region. Drought is important for the climate studies of that region.

The lack of rainfall in a region does not necessarily indicate drought. Drought is defined as a prolonged period of time without precipitation, according to climatology. Drought is a climate phenomenon that can recur. Droughts can occur anywhere in the world, regardless of the season. Unlike other

[1] Assoc. Prof. Dr., (Kafkas University/ Faculty of Engineering and Architecture/ Civil Engineering Department), emretopcu01@gmail.com, ORCID: 0000-0003-0728-7035.

[2] Research Assistant., (Kafkas University/ Faculty of Engineering and Architecture/ Civil Engineering Department), fatihkaracor@gmail.com, ORCID: 0000-0003-1201-7857.

natural disasters, droughts develop slowly and persist for extended periods.

Drought is usually analyzed in 4 categories. These are: Meteorological drought, hydrological drought, agricultural drought and socioeconomic drought.

**Meteorological Drought:** The occurrence of any category of drought starts with the lack of rainfall in that region. Meteorological drought is primarily associated with a lack of rainfall. When the rainfall deficit in a region is much less than its long-term climatological average (usually at least 30 years), the resulting drought is defined as meteorological drought.

**Agricultural Drought:** Reduced water supply from both meteorological and hydrological sources reduces the irrigation water needed to grow crops. This irrigation water needs to be stored in the soil as soil water. However, soil water is also affected by drought at the highest level. Continuous dry weather leads to a lack of moisture and reduces the water resources needed for agriculture. As a result, agricultural drought occurs as the lack of water in the soil affects crop stress and crop availability.

**Hydrological Drought:** It is recognized that hydrological drought occurs due to the decrease in surface water resources, decrease in flow values and drying of lakes due to prolonged lack of precipitation. It can be decided whether there is a drought with stream flow measurements, lake, reservoir, groundwater level measurements. Since there is a certain time interval between the lack of precipitation and the lack of water in rivers and reservoirs, we cannot immediately say that there is drought as a result of hydrological measurements. Hydrological drought follows agricultural drought and results in a significant reduction in groundwater and river levels.

**Socioeconomic Drought:** Drought is not just a temporary natural disaster. It has negative impacts on society due to the

imperative need of people and all kinds of work they do for water reserves. Socioeconomic drought is a type of drought that occurs as a result of the inability to meet the water needs of societies and industry due to the drying up and unusability of water resources that will meet the water demand.

Drought is not only the result of a lack of rainfall. Ever since the formation of water on earth, the amount of water has been constant and in constant motion. This movement is caused by the Sun, which is called an infinite source of energy, and its effects on the earth. Under the influence of the Sun, the continuous movement of water between the atmosphere and the earth is called the "hydrological cycle (water cycle)". Any deterioration or deviation from normal in any of the parameters that make up the hydrological cycle such as solar radiation, evaporation, evapotranspiration, cloud condensation, wind, surface and underground flow can cause drought. In short, all climatic, meteorological, and hydrological events can trigger drought. In order to make an accurate drought analysis, the elements of the hydrological cycle should be monitored regularly and the tendency of deviations from their normal state should be followed.

The aim of this study is to conduct a comprehensive drought analysis using various meteorological parameters of 4 observational points (Büyükçekmece, Beykoz, Sabiha Gökçen Airport and Şile) in Istanbul, the most populous and industrially developed city of Turkey. The drought analysis in the study was performed with the Composite Drought Index obtained by using the Standardized Precipitation Evapotranspiration Index using precipitation and temperature parameters; AGGREGATE Drought Index using humidity, wind speed, AO, NAO, SOI and sunspot number; and Water Storage Deficit Index using terrestrial water storage values. Drought was analyzed in 3, 6 and 12-month

periods. The period between 2003 and 2021 was analyzed in terms of drought.

## 2. MATERIAL AND METHOD

### 2.1.Material

All of the meteorological parameters used in the study were obtained from sources that make measurements using remote sensing method. The sources of the obtained parameters are briefly described below.

The Prediction of Worldwide Energy Resources (POWER) application, provided by the National Aeronautics and Space Administration (NASA), offers data on monthly total precipitation, monthly average temperature, monthly average relative humidity, and monthly average wind speed parameters. The available data maintains the source spatial resolution. NASA's objective in Earth science is to observe, comprehend, and model the Earth system to determine changes, predict them more accurately, and understand their impact on life on Earth. The Science Mission Directorate's Applied Sciences Program serves NASA and society by accelerating the realization of societal and economic benefits from Earth science, information, and technology research and development. The Prediction Of Worldwide Energy Resources (POWER) project was established to enhance the existing renewable energy dataset and create new datasets from recently launched satellite systems. The POWER project caters to three user communities: Renewable Energy, Sustainable Buildings, and Agroclimatology (NASA POWER, 2024).

The values for terrestrial water storage deficit were obtained from the NASA GRACE application. The twin GRACE satellites, launched on 17 March 2002, provide precise

measurements of variations in Earth's gravitational field. This has revolutionised research into Earth's water reserves over land, ice, and oceans, as well as seismic activity and crustal deformations (NASA GRACE, 2024). The Gravity Recovery and Climate Experiment (GRACE) was a joint mission of NASA and the German Aerospace Center (DLR). From March 2002 to October 2017, twin satellites measured Earth's gravity field anomalies. The mission is sometimes referred to as Tom and Jerry, in reference to the famous cartoon. In May 2018, the GRACE Follow-On (GRACE-FO) was launched as a continuation of the mission, using near-identical hardware (Wikipedia, 2024a).

Spots are dark areas in the Sun's photosphere that are caused by intense magnetic flux from the Sun's inner core. The upper photosphere and chromosphere along this magnetic flux heat up and are typically visible as faculae and plage, which are often referred to as active regions. Sunspot values (https://www.sidc.be/SILSO/datafiles) retrieved from the internet source.

The North Atlantic Oscillation (NAO) is a phenomenon in the North Atlantic Ocean. At the poles, a high pressure area is formed at sea level with low heat energy due to the narrowing angle of the sun's rays, while in the equatorial regions, on the contrary, a low pressure area is formed with high heat energy. The positive and negative states of the NAO index directly affect the countries on the Atlantic coast meteorologically. Countries like Turkey are indirectly affected by the NAO index, with a minimum effect in summer and a maximum effect in winter (Wikipedia, 2024b). Arctic Oscillation (AO) is a type of index based on the pressure anomalies observed from 20 degrees above the latitudes of the Northern Hemisphere (Wikipedia, 2024c). The SOI is an index, derived from the difference in sealevels (SLPs) between Tahiti and Darwin, Australia. It is used to monitor what is known as the state of the Southern Oscillator, the variations in

air pressure that occur between the western and eastern tropical Pacific during El Niño and La Niña episodes (NOAA, 2024).

The geographical characteristics of the observational points used in the study are shown in Table 1. The location of the study area in Turkey is shown in Figure 1.

**Table 1. Geographical feautres of observational points**

| Observational point name | Elevation (m) | (Latitude) N | (Longitude) E | Period |
|---|---|---|---|---|
| Sabiha Gökçen Airport | 99 | 40.8977 | 29.3033 | 2003-2021 |
| Şile | 83 | 41.1688 | 29.6007 | 2003-2021 |
| Büyükçekmece | 20 | 41.0453 | 28.5900 | 2003-2021 |
| Beykoz | 5 | 41.1417 | 29.0739 | 2003-2021 |

**Figure 1. Location of the observational points in Turkey**

## 2.2. Method

### 2.2.1. Standardized Precipitation Evapotranspiration Index (SPEI)

Vicente-Serrano et al. (2010) developed the SPEI method, which is a more comprehensive drought analysis method than the widely used Standardized Precipitation Index (SPI) (Mckee et al., 1993; Topçu and Karaçor 2023). Unlike SPI, which only considers precipitation, SPEI takes into account both temperature and precipitation parameters. The Standardised Precipitation Evapotranspiration Index (SPEI) is calculated in the same way as the SPI and represents the climate balance. and represents the water balance of the climate by measuring the variance between the monthly precipitation and the potential evapotranspiration (PET). The initial step in SPEI calculation is determining PET. For this study, the Thornthwaite method, a simple PET calculation method, was employed.

The Thornthwaite method, proposed by Thornthwaite (1948), is widely used to estimate potential evapotranspiration (PET). This method assumes that PET does not occur at temperatures of 0°C and below. As the study station also experiences temperatures of 0°C and below during the winter months, PET values during these months were considered as 0. Equation 1 is used to estimate PET.

$$\mathrm{PET} = 16.\left(\frac{\mathrm{N}}{12}\right).\left(\frac{\mathrm{m}}{30}\right).(10.\frac{\mathrm{T_{mean}}}{\mathrm{I}})^{\mathrm{a}} \quad (1)$$

$T_{mean}$ monthly average temperature (°C), N monthly average daylight hours (hours/day), m number of days in each month, I heat index, a coefficient is found with the help of Equation 2 below.

$$a = 6.75 \times 10^{-7} \times I^3 - 7.71 \times 10^{-5} \times I^2 + 1.79 \times 10^{-2} \times I + .049 \quad (2)$$

Finally, the heat index I is found as the sum of 12 monthly values as in Equation 3.

$$I = \sum_{i=1}^{12} \left(\frac{T_{imean}}{5}\right)^{1.514} \quad (3)$$

The difference between cumulative monthly precipitation (P) and monthly evapotranspiration (PET) is calculated using Equation 4.

$$D_i = P_i - PET_i \quad (4)$$

The cumulative water gain or loss in meteorological terms at different time intervals is obtained using Equation 5.

$$D_n^k = \sum_{i=0}^{k-1} (P_{n-i} - PET_{n-i}), \qquad n \geq k \quad (5)$$

Where k is the time interval (months) and n is the accounting frequency.

The calculation of SPEI requires a 3-parameter distribution, unlike SPI. Vicente-Serrano found that the three-parameter log-logistic fit the D-series better than the Pearson III, log-normal and generalized extremes. For this reason, the log-logistic probability density function is used, as determined by equation 6.

$$f(x) = \frac{\beta}{\alpha}\left(\frac{x-\gamma}{\alpha}\right)^{\beta-1}\left[1 + \left(\frac{x-\gamma}{\alpha}\right)^{\beta}\right]^{-2} \quad (6)$$

α, β and γ are the scale, shape and origin parameters respectively. They are obtained separately with the help of L-moments (Equations 7, 8 and 9).

$$\beta = \frac{2\omega_1 - \omega_0}{6\omega_1 - \omega_0 - 6\omega_2} \quad (7)$$

$$\alpha = \frac{(\omega_0 - 2\omega_1)\beta}{\Gamma\left(1+\frac{1}{\beta}\right)\Gamma\left(1-\frac{1}{\beta}\right)} \quad (8)$$

$$\gamma = \omega_0 - \alpha\Gamma(1 + \tfrac{1}{\beta})\Gamma(1 - \tfrac{1}{\beta}) \quad (9)$$

Here $\Gamma(1+\frac{1}{\beta})$ is the gamma function of $(1+\frac{1}{\beta})$ and $\omega_s$ is the s-order probability density function calculated as in Equation 10, taking the values s= 0, 1, 2.

$$\omega_s = \frac{1}{n}\sum_{i=1}^{n}(1-\frac{j-0.35}{n})^s D_i \quad (10)$$

Where n is the number of data points and j is the observation interval in ascending order.

Eq. 11 gives the logarithmic probability density function for the *D* series.

$$F(x) = \left[1+(\frac{\alpha}{x-\gamma})^{\beta}\right]^{-1} \quad (11)$$

The SPEI value is calculated as the standardized value of $F(x)$ as in Equation 12.

$$SPEI = W - \frac{c_0+c_1W+c_2W^2}{1+d_1W+d_2W^2+d_3W^3} \quad (12)$$

$$W = \sqrt{-2\ln(P)} \text{ for } P \leq 0.5 \quad (13)$$

*P* in Equation 13 indicates the probability of exceeding a specified value of *D*.

$P = 1 - F(x)$; $P > 0.5$, $P = 1 - P$ and the constants are as shown below;

$c_0$=2.515517,

$c_1$=0.802853,

$c_2$=0.010328,

$d_1$=1.432788,

$d_2$=0.189269,

$d_3$=0.001308 (Yang et al., 2016)

### 2.2.2. Aggregate Drought Index (ADI)

Aggregate Drought Index (Keyantash and Dracup, 2004). We can say that one meteorological parameter can influence the occurrence of another meteorological parameter, especially when the hydrological cycle is considered, which can be reflected in the drought in the region.

Principal Component Analysis (PCA) is a transformation technique that helps to reduce the size of data series containing interrelated parameters, such as in the Aggregate Drought Index, to fewer dimensions while preserving the changes that occur within the data set. The aim here is to express the data set with fewer variables. Principal Component Analysis requires the construction of a square symmetric R matrix that describes the correlation between the original data set. To calculate the principal components:

From the obtained parameters, a data matrix is created for each month of each hydrological year. In this matrix, each column represents a data (precipitation, evaporation, runoff, etc.). O (observed values) is the matrix of observed values. The O matrix in Equation 14 is created in N x p dimension. N is the number of hydrological years used in the calculation and p is the number of parameters.

$$O = \begin{bmatrix} \text{AO} & \text{NAO} & \text{SOI} & \text{Sunspot number} & \text{Humidity} & \text{Wind velocity} \\ : & : & : & : & : & : \\ : & : & : & : & : & : \\ : & : & : & : & : & : \\ : & : & : & : & : & : \end{bmatrix} \quad (14)$$

As a second step, each column is standardized by subtracting its mean and dividing by its standard deviation (the X matrix is obtained). This is because it is desirable that the observed values used are not weighted in the results.

In the third step, the correlation matrix (R) of the matrix created from the standardized data set is created. In this way, the

relationship of each parameter with each other is obtained. For each month, 12 different correlation matrices need to be created. Where R is the correlation matrix and X is the standardized observation matrix, the correlation matrix (R) of the observed data matrix is found as in Equation 15. The transpose of the standardized matrix is $X_T$. N is the number of hydrological years calculated.

$$R = \frac{1}{N-1} X^T X \quad (15)$$

PCA is conducted on the correlation matrix (R) that was obtained. In this way, the eigenvectors and eigenvalues of the matrix are found. The eigenvectors allow to calculate the uncorrelated principal component, which is a standardized linear combination of the original variables. The eigenvalues measure the amount of variation explained by each principal component. Since the correlation matrix is used to construct the Aggregate Drought Index, the index values are not affected by the units of the parameters. Each parameter can be used in its own unit. Since the ADI is constructed by the principal component analysis method, its difference from other drought indices stems from this, and it is in the category of very powerful and comprehensive drought indices. If the principal components matrix is called Z, the standardized observation data matrix is called X, and the eigenvector matrix obtained from the correlation matrix (R) is called E, Z=XE.

$ADI_{ik}$ is the Aggregate Drought Index value for month k in year i, $Z_{ik}$ is the first principal component for month k in year i, σ is the standard deviation of the first principal component for month k in all hydrological years as in Equation 16. In the calculation of the ADI, only the first principal component is taken into account. This is because it explains most of the parameter variation in the entire standardized dataset.

$$ADI_{ik} = (Z_{ik})/\sigma \quad (16)$$

After obtaining $ADI_{ik}$ values, Aggregate Drought Index (ADI) values are obtained by serializing each month of the hydrological years. ADI values are calculated for a period of 12 months. In ADI method, there is no definite drought category as in SPI or SPEI methods. In SPI, threshold values of 0, -1, -1.5 and -2 correspond to cumulative probability values of 0.5, 0.1587, 0.0668 and 0.0228, respectively. In ADI, boundary values corresponding to these cumulative probability values were determined.

### 2.2.3. Water Storage Deficit Index (WSDI)

Obtained from monthly GRACE TWSA deviations, WSDI is employed to characterize drought formations and severity of drought (Yirdaw et al., 2008). WSDI is obtained with the help of Equation 17 and Equation 18.

$$WSD_{i,j} = TWSA_{i,j} - \overline{TWSA_{j}}, \quad (17)$$

$$WSDI_{i,j} = \frac{WSD_{i,j} - \mu}{\sigma} \quad (18)$$

For the j[th] month in year i, $WSD_{i,j}$ and $TWSA_{i,j}$ represent the total water storage deficit and GRACE-inferred TWSA time series, respectively. The long-term TWSA average for the same month is represented by $\overline{TWSA_{ji}}$.

μ and σ are the mean and standard deviation of the WSD timeseries. WSDI values below zero indicate a deficit in total water storage, while values above zero indicate a surplus.

### 2.2.4. Composite Drought Index (CDI)

One index alone cannot capture the drought event accurately. Hence, we build an CDI using the SPEI, WSDI and ADI by means of a weighted linear combination, namely.

$$CDI = a.SPEI + b.WSDI + c.ADI \quad (19)$$

The monthly CDI is equivalent to the SPEI, the WSDI and the ADI. Coefficients a, b, and c represent each index's contribution to CDI scores. As different regions experience different types of drought, there is some flexibility in these factors. Coefficients a, b, and c are also based on a composite meteorological index calculation procedure, which has been accepted in China's national standards and applied in various researches (for instance Wang et al., 2014).

$$a = \frac{a_1}{m}, b = \frac{b_1}{m}, c = \frac{c_1}{m} \quad (20)$$

Here $m = a_1 + b_1 + c_1$ and $a_1$, $b_1$ and $c_1$ are the ratios of the average value for moderate dryness (value <-1.0) divided by the corresponding minimum value. $a_1$ can be calculated as;

$$a_1 = \frac{mean\ (drought\ index_1{}')}{\min(drought\ index_1)} \quad (21)$$

where $drought\ index_1{}'$ is the corresponding value of d$rought\ index_1$, i.e. less than -1. In Equation (21), $drought\ index_1$ stands for SPEI, WSDI or ADI.

## 3. RESULTS AND DISCUSSION

The results obtained as a result of the analyses carried out in the study were visualized in graphs and tables. In the study, drought analysis was carried out for 3, 6 and 12-month periods. While the 3 and 6-month periods represent short-term drought, the 12-month period represents long-term drought. While the traces of meteorological drought can be seen in the short term, the symptoms of hydrological drought appear in the long term. For this reason, drought was analyzed for 3 different periods. SPEI, WSDI and ADI values were obtained. However, since the main purpose of the study is to interpret the results with CDI, SPEI, WSDI and ADI results are not included in this section.

Table 2 shows the values of the observational points corresponding to drought categories for CDI. These thresholds are extreme wet, very wet, moderately wet, normal, moderately dry, very dry and extreme wet from wet to dry. Each observational point has its own drought thresholds. Someone looking at Table 2 can recognize which drought category is experiencing drought by reading the CDI values obtained according to the values in the table. For example, at the Büyükçekmece observational point, a value between 0.98 and 1.30 for the 3-month period indicates severe wet. Values greater than 1.30 represent extreme wet conditions. At the Beykoz observational point, CDI values less than -1.32 for the 6-month period indicate that extreme drought was experienced. Again in Beykoz, values less than -0.99 for a 12-month period indicate extreme drought. At Sabiha Gökçen Airport, values between -1.08 and -1.44 in a 3-month period mean severe drought. In Şile, values less than -0.96 in the 12-month period indicate extreme drought conditions. In the 6-month period, values greater than 1.38 indicate extreme wet conditions. Normally SPEI drought categories are fixed, i.e. there are predetermined thresholds for each study point. Similarly, WSDI has similar drought thresholds as SPEI. However, since ADI is also used in the calculation of CDI and there are no fixed thresholds for ADI, CDI also does not have fixed drought thresholds. Therefore, Table 2 shows different values for each observational point.

Figure 2 shows the change graphs of CDI values according to months for each observational point. The vertical axis shows the CDI values and the horizontal axis shows the months. Looking at this graph, one can see that CDI values increase or decrease from month to month. The near normal values in Table 2 are approximately 0 for the 3, 6 and 12 month periods and values below this value indicate the onset of drought. The 0 axis is drawn in red. Looking at the graphs in Figure 2, it

can be said that dry periods are followed by wet periods and wet periods are followed by dry periods. Again, according to Figure 2, it can be said that Sabiha Gökçen Airport is the observational point where the most severe drought is experienced.

**Table 2. CDI values of observational points for drought category**

| | **BÜYÜKÇEKMECE CDI** | | |
|---|---|---|---|
| | **3 month** | **6 month** | **12 month** |
| Extreme wet | 1.30 | 1.37 | 1.13 |
| Severe wet | 0.98 | 1.04 | 0.86 |
| Moderate wet | 0.66 | 0.70 | 0.60 |
| Normal | 0.01 | 0.03 | 0.07 |
| Moderate drought | -0.63 | -0.64 | -0.46 |
| Severe drought | -0.95 | -0.98 | -0.73 |
| Extreme drought | -1.27 | -1.31 | -0.99 |
| | **BEYKOZ CDI** | | |
| | **3 month** | **6 month** | **12 month** |
| Extreme wet | 1.32 | 1.38 | 1.13 |
| Severe wet | 0.99 | 1.04 | 0.86 |
| Moderate wet | 0.67 | 0.70 | 0.60 |
| Normal | 0.02 | 0.03 | 0.07 |
| Moderate drought | -0.63 | -0.64 | -0.46 |
| Severe drought | -0.96 | -0.98 | -0.72 |
| Extreme drought | -1.28 | -1.32 | -0.99 |
| | **SABİHA GÖKÇEN AIRPORT CDI** | | |
| | **3 month** | **6 month** | **12 month** |
| Extreme wet | 1.46 | 1.46 | 1.22 |
| Severe wet | 1.10 | 1.10 | 0.93 |
| Moderate wet | 0.74 | 0.75 | 0.65 |
| Normal | 0.01 | 0.03 | 0.08 |
| Moderate drought | -0.72 | -0.68 | -0.49 |
| Severe drought | -1.08 | -1.04 | -0.78 |
| Extreme drought | -1.44 | -1.39 | -1.06 |
| | **ŞİLE CDI** | | |
| | **3 month** | **6 month** | **12 month** |
| Extreme wet | 1.34 | 1.38 | 1.10 |
| Severe wet | 1.01 | 1.05 | 0.84 |
| Moderate wet | 0.68 | 0.71 | 0.58 |
| Normal | 0.02 | 0.04 | 0.07 |
| Moderate drought | -0.63 | -0.63 | -0.45 |
| Severe drought | -0.96 | -0.97 | -0.70 |
| Extreme drought | -1.29 | -1.31 | -0.96 |

**Figure 2. CDI graphs of observational points**

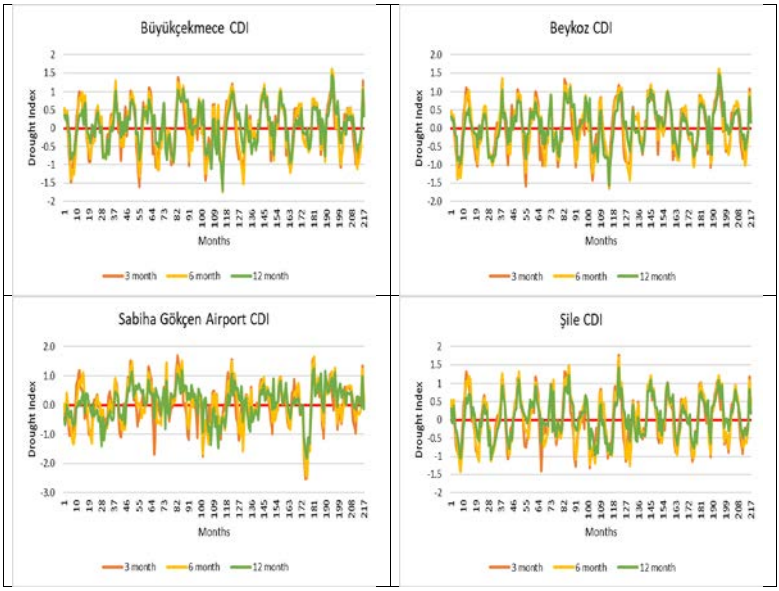


**Table 3. Extreme CDI values of observational points**

| **BÜYÜKÇEKMECE CDI** | | | | | | | | |
|---|---|---|---|---|---|---|---|---|
| **3 month** | | | **6 month** | | | **12 month** | | |
| Min. | -1.62 | 2012, September | Min. | -1.73 | 2012, September | Min. | -1.71 | 2012, September |
| Mak. | 1.39 | 2010, January | Mak. | 1.61 | 2019, April | Mak. | 1.43 | 2019, April |
| **BEYKOZ CDI** | | | | | | | | |
| **3 month** | | | **6 month** | | | **12 month** | | |
| Min. | -1.59 | 2012, September | Min. | -1.64 | 2012, September | Min. | -1.56 | 2012, September |
| Mak. | 1.35 | 2006, April | Mak. | 1.62 | 2019, April | Mak. | 1.46 | 2019, April |
| **SABİHA GÖKÇEN AIRPORT CDI** | | | | | | | | |
| **3 month** | | | **6 month** | | | **12 month** | | |
| Min. | -2.52 | 2017, September | Min. | -2.46 | 2017, October | Min. | -1.83 | 2017, October |
| Mak. | 1.68 | 2010, February | Mak. | 1.63 | 2018, March | Mak. | 1.24 | 2018, March |
| **ŞİLE CDI** | | | | | | | | |
| **3 month** | | | **6 month** | | | **12 month** | | |
| Min. | -1.41 | 2008, August | Min. | -1.43 | 2003, October | Min. | -1.08 | 2005, August |
| Mak. | 1.76 | 2013, April | Mak. | 1.70 | 2013, April | Mak. | 1.42 | 2013, April |

Table 3 shows the maximum and minimum CDI values for each observational point, the years and months of occurrence. For example, at Büyükçekmece station, the minimum CDI values were observed in September 2012 for all 3 periods. While the

maximum values were observed in January 2010 for the 3-month period, they were observed in April 2019 for the 6 and 12-month periods. In Beykoz, minimum CDI values were observed in the same year and month as Büyükçekmece. Maximum values were observed in the same year and month as Büyükçekmece in the 6 and 12-month periods, while the 3-month period was observed in April 2006. At Sabiha Gökçen Airport, the minimum values were observed in September 2017 in the 3-month period and in October 2017 in the 6 and 12-month periods. Finally, maximum values in Şile were observed in April 2013 in all 3 periods. The minimum CDI values representing extreme drought were observed in August 2008 in the 3-month period, October 2003 in the 6-month period, and August 2005 in the 12-month period.

Figure 3 shows graphs of drought frequency values in percentages corresponding to drought categories. In these graphs, drought frequency values can be seen for 3, 6 and 12-month periods. Based on these graphs, it can be said that near normal conditions are experienced the most and extreme wet and extreme drought conditions are experienced the least. In Büyükçekmece, the extreme drought frequency obtained in the 3 and 6-month periods is 4%, while it is 2% in the 12-month period. In Sabiha Gökçen Airport, the frequency of both extreme wet and extreme drought conditions is higher than the other observational points.

**Figure 3. Drought frequency (%) values of observational points according to drought thresholds**

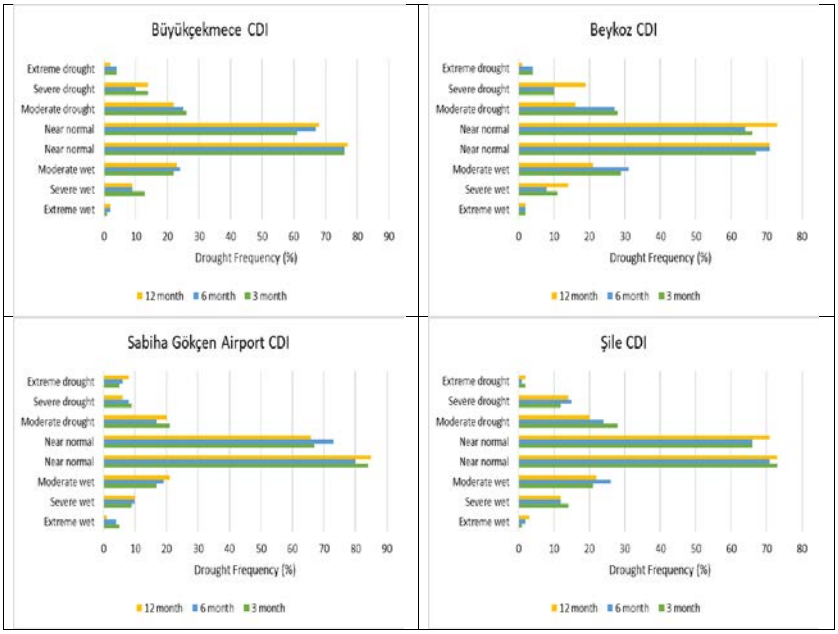


## 4. CONCLUSION

In this study, a comprehensive drought analysis of 4 observational points in Istanbul was carried out with the help of Composite Drought Index (CDI). The parameters that form and affect the hydrological cycle were tried to be used. SPEI, WSDI and ADI were used to calculate the CDI. Specific drought thresholds were determined for each observational point. Drought frequency values corresponding to these thresholds were obtained. The results are presented in tables and graphs.

According to the findings, extreme drought and extreme wet events can be observed at the observational points. However, near normal conditions are observed the most. Extreme values are most frequently observed at Sabiha Gökçen Airport. Very long lasting wet or drought conditions were not observed in the region.

Wet and drought conditions follow each other. The climatic indices and sunspot number used in this study have of course influenced the analysis results. These parameters can disrupt the balance of wet and drought conditions on the earth's surface. The study area is therefore also affected. The results of the analysis also revealed the changes occurring in the region within the framework of global climate change. Especially after 2010, extreme conditions have manifested themselves. Since the region is very developed in terms of population and industry, some measures should be taken by the authorities to reduce the symptoms of global climate change.

Since drought analysis with CDI has not been done before in the region, a different perspective has been brought to the arid and wet conditions in the region. This study is expected to be a hydrological resource for water resources engineers, planners and responsible authorities in the region.

**REFERENCES**

Keyantash A.J., Dracup A.J., "An aggregate drought index: Assessing drought severity based on fluctuations in the hydrologic cycle and surface water storage", Water Resources Research, Vol 40, W09304, (2004)

Mckee T. B., Doesken N. J., and Kleist J., "The Relationship of Droght Frequency and Duration to Time Scales", Reprints, 8th Conference on Applied Climatalogy, Anaheim, CA, USA, 179–184 p.,(1993)

NASA GRACE, 2024, (https://grace.jpl.nasa.gov/mission/grace/) Access date: 2024/03/01.

NASA POWER, 2024, ( https://power.larc.nasa.gov/). The data was obtained from the POWER Project's monthly 2.0.0 version on 2024/03/01

NOAA, 2024, https://www.ncei.noaa.gov/access/monitoring/enso/soi, Access date 2024/03/01

Thornthwaite C.W., "An approach toward a Rational Classification of climate". Geographical Review, 38 (1), 55e94, (1948).

Topçu, E., & Karaçor, F. (2023). A comparative investigation on the applicability of the actual precipitation index (API) with the standardized precipitation index (SPI): the case study of Aras Basin, Turkey. Theoretical and Applied Climatology, 154(1-2), 29-42.

Vicente-Serrano S.M., Beguería, S., López-Moreno J.I. "A multiscalar drought index sensitive to global warming: The standardized precipitation evapotranspiration index", J. Clim. 23, 1696–1718, (2010)

Wang X, Hou X, Li Z, Wang Y. 2014. Spatial and temporal characteristics of meteorological drought in Shandong Province, China, from 1961 to 2008. Advances in Meteorology 2014: 1–11. DOI: 10.1155/2014/873593

Wikipedia, 2024a. (https://en.wikipedia.org/wiki/GRACE_and_GRACE-FO). Access date: 2024/03/01.

Wikipedia, 2024b, (https://tr.wikipedia.org/wiki/Kuzey_Atlantik_salınımı). Access date 2024/03/01

Wikipedia, 2024c, (https://tr.wikipedia.org/wiki/Arktik_salınım). Access date 2024/03/01

Yang M., Yan D., Yu Y., Yang Z., "SPEI-Based Spatiotemporal Analysis of Drought in Haihe River Basin from 1961 to 2010". Hindawi Publishing Corporation Advances in Meteorology Volume, Article ID 7658015, 10 pages, (2016)

Yirdaw, S.Z., Snelgrove, K.R., & Agboma, C. O. (2008). GRACE satellite observations of terrestrial moisture changes for drought characterization in the Canadian Prairie. J. Hydrol. 356, 84–92.

# İNŞAAT MÜHENDİSLİĞİ ALANINDA AKADEMİK

# ANALİZLER

**YAZ Yayınları**
**M.İhtisas OSB Mah. 4A Cad. No:3/3**
**İscehisar / AFYONKARAHİSAR**
**Tel : (0 531) 880 92 99**
**yazyayinlari@gmail.com • www.yazyayinlari.com**

**ISBN: 978-625-6642-32-4**